Qualitative assessment of laser-induced breakdown spectra generated with a femtosecond fiber laser

Huan Huang,* Lih-Mei Yang, and Jian Liu

PolarOnyx, Inc., 2526 Qume Drive, Suite 17 & 18, San Jose, California 94538, USA

*Corresponding author: hhuang@polaronyx.com

Received 5 October 2012; revised 19 November 2012; accepted 20 November 2012; posted 20 November 2012 (Doc. ID 176453); published 17 December 2012

This paper presents what is to our knowledge the first evaluation of laser-induced breakdown spectroscopy (LIBS) studies on elemental composition detection and identification by employing a femtosecond (fs) fiber laser. Qualitative LIBS spectra were obtained in ambient air using a 1030 nm fs fiber laser. Specific ion and neutral emission lines of different materials have been characterized, including metal, metal alloy, semiconductor, and glass. The performance and LIBS spectra of an intensified CCD (ICCD) system and a nonintensified CCD system were compared. Time-resolved emission spectra depicting the detailed plasma evolution was collected from sub-spot-size craters. The gated ICCD gives improved signal-to-noise ratio by a factor of 20 compared with a nongated, nonintensified CCD system. This shows a potential portable and field-deployable LIBS system for versatile and rapid analysis of chemicals and special materials.

OCIS codes: 060.3510, 300.6365, 140.3440.

1. Introduction

Laser-induced breakdown spectroscopy (LIBS) has been rapidly developed as a versatile and attractive analytical method over the past two decades. It has the primary advantages of versatile sampling, little to no sample preparation, sensitivity to a wide variety of elements, and rapid and simultaneous analysis of multi-elements, and it is practically nondestructive. LIBS has been applied to the analysis of a number of materials including metals [1–5], polymers [6], biological matter [7–9], gases [10,11], and explosive materials [12–15]. The laser sources typically used are traditional solid state Nd:YAG lasers with nanosecond (ns) pulse duration and the pulse energy is above the 1 mJ level. Although LIBS analysis with high spatial resolution was achieved for metals [4,5], sub spot size ablation is hard to obtain due to the longer laser pulse duration and thermal diffusion. Furthermore, the ns laser source has certain less than desirable features, such as broadband background emission and matrix effects, which lead to undue pulse to pulse variation. Although this limitation can be addressed through the use of the double pulse approach, including both the ns–ns [16,17] and fs–ns combinations [18], it also increases system size and weight. The ns laser source also extends plasma lifetime and mixing of ambient air with the sample leading to compromised H, O, and N atom emissions, so it may not be a proper measurement source for detecting trace explosives where the nitrogen to oxygen ratios are key indicators of highly oxidized/explosives compounds. Another disadvantage of the LIBS processes with a long pulsed laser is the large heat-affected zone as a result of linear absorption of laser energy.

In recent years, researchers have demonstrated that fs-LIBS reduces the matrix effect by yielding more reproducible ablation and the microplasma phenomenon is too short to allow for mixing with ambient air [1, 19,20]. For fs lasers, lower energies are needed for ablation compared with ns pulses due to its shorter pulse duration, less damage to surrounding materials, and less ablation of material being analyzed by the laser spark. The significant lower background emissions from the ablation-induced plasma by fs

1559-128X/12/368669-08$15.00/0

lasers have been reported by several groups and have been attributed to lack of plasma reheating [1,2,7,8,15,21,22]. Compared with ns laser pulses, fs lasers make it possible to obtain sub-spot-size or even nanometer size ablation due to the unique feature of a sharply defined threshold for optical breakdown [2,8] and a potential for better spatial resolved LIBS results. Furthermore, use of an fs laser is beneficial for providing sufficient momentum for a collision dominated breakdown process and an improved LIBS signal-to-noise ratio (SNR) [1,2,8,19]. Therefore, fs lasers provide a LIBS process with a lower ablation threshold and an improved spatial resolution and SNR.

General laboratory solid state fs lasers tend to be large, complicated, and expensive. New and innovative technology developments are required to develop fs laser sources suitable for portable and field-deployable fs-LIBS applications. In particular, fs fiber lasers appear to show considerable potential and advantages over solid state lasers, such as compactness, high performance (more reliable and maintenance-free), high repetition rate, and low cost for field-deployable LIBS systems. Few LIBS studies have been reported using fiber lasers [23,24]. To the authors' knowledge, the present study is the first assessment of LIBS spectra using an fs fiber laser.

In this study, a LIBS system based on an fs fiber laser was used to study elemental composition. LIBS spectra were obtained using a near-infrared (1030 nm) fs fiber laser. Atomic emission lines of different materials have been characterized, including metal, metal alloy, semiconductor, and glass. Different laser processing parameters including laser pulse energy and scanning speed have been investigated to study its influence. Furthermore, the performance and LIBS spectra of an intensified CCD (ICCD) system and a nonintensified CCD system are compared. It is shown that with delay and gating control, the SNR can be greatly enhanced.

2. Methods and Materials

A. Experimental Setup

Figure 1 shows the LIBS experimental setup in this study. The fs fiber laser system is a commercialized mode-locked seed fiber laser (PolarOnyx, Inc., Uranus Series). The output laser beam has a 750 fs pulse duration (FWHM), 1030 nm center wavelength, pulse repetition rate tunable between 1 Hz and 1 MHz, and pulse energy up to 10 μJ. The output collimated beam is a nearly symmetric Gaussian beam with $M^2 < 1.3$. The laser beam is focused onto the sample by microscope objectives. Two infinity corrected focusing objectives are alternatively used: 50× (NA = 0.55) and 20× (NA = 0.4). A smaller focal spot diameter of about 5 μm was achieved by the larger NA objective. An attenuator is used to control the laser pulse energy and a mechanical shutter is synchronized with the laser system. The total beam delivery loss is less than 20 percent. The sample is mounted on a motorized three-dimensional translation stage and the motion stage is

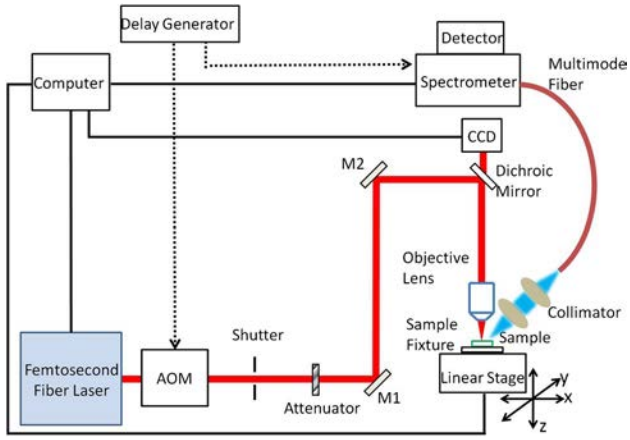

Fig. 1. (Color online) Femtosecond fiber LIBS experimental setup.

controlled by computer to achieve different moving sample speeds. The sample surface is adjusted perpendicular to the laser beam. Special care is taken to keep the laser focus on the sample for every ablation spot—a relatively lower pulse energy (close to the ablation threshold of the material) is used to generate single shot ablation, and the focal position is finely adjusted until the ablation just starts, after that higher pulse energy can be used for LIBS experiment analysis. During the experiments, the target samples are moving in the transverse direction (y axis) with the motion stage and the translation speed is from 0.1 mm/s to 100 mm/s. During the experiment, a step increase will be added so that fresh sample surfaces will always be ablated for LIBS signal collection. Pulse overlap may appear for each ablation spot along the scanning path depending on the scanning speed and repetition rate. A constant air flow is placed across the sample surface during the experiment to flush out the plume of ablated and re-condensed material and the air exchange rate is estimated about 10 $L/$ min.

B. Materials

In this study, different bulk metals (aluminum), metal alloys (lead–tin alloy and brass), semiconductor (gallium arsenide), and glass (soda lime glass) were used. The bulk target surfaces were carefully cleaned before the experiments. No quantification was attempted for this experiment.

C. LIBS Signal Collection

Generally, spectrometer and detector choices for LIBS depend on many factors, including type of laser processing (single-shot or multi pulses averaging), required sensitivity, spectral bandwidth, field deployability, and cost. Two spectrographs and detectors were used here depending on the experimental requirements. The specifications of the two detectors are listed in Table 1. An important characteristic of the emitting plasma induced by fs laser pulses is related to the absence of interactions between the laser beam and the formed expanding plasma. This effect

Table 1. LIBS Signal Collection Systems Specifications

Spectrometer and Detector Model	Ocean Optics QE65000	Andor Technology—iStar ICCD
Resolution	1.9 nm	Wavelength dependent ($\lambda/\Delta\lambda = 6000$)
Grating	HC1-QE	1200 g/mm
Active pixels	1024 × 58	1024 × 1024
Pixel size	24.576 μm^2	13.6 μm^2
Entrance slit width	25 μm	50 μm
CCD cooling	−30°C	−30°C
Intensifier	No	Gen 2
Gating	No	5 ns

provided a background continuum lower than those induced by ns laser pulses, which can be considered an advantage in order to obtain good analytical results even without gated detectors [7,15]. However, the characteristic emission intensity is also lower in detection, so multiple pulse accumulation is used. For a nonintensified detector, the LIBS signal was collected by line scanning the sample with pulse overlapping effect. The integration time is properly selected to obtain good spectrums based on different laser parameters and plasma intensity level; for intensified detector, single-shot ablation was used and multiple shots accumulation was collected to avoid sample-to-sample variation. A delay generator (Stanford Research DG 535) is used for synchronization and delay generation. The optical emission from the ablation was collected by a collimator lens, and then coupled into a multimode optical fiber and delivered to a spectrometer. The collection optics is oriented at about 30 deg above the processing location. An optional filter was used during the experiment to block the laser wavelength. All the experiments were conducted in ambient air.

For quantitative estimation, the SNR was calculated and defined as the ratio of the integrated atomic emission line intensity (peak area) to the average peak noise. The average peak noise was calculated by use of the rms of the adjacent, featureless continuum intensity times the full peak width.

3. Results and Discussion

At first, line scanning and a nonintensified detector were used and the emitted plasmas, by overlapped multiple pulse interactions, were collected and averaged for characteristic analysis. For each individual spectrum, a fresh surface of the sample was presented and scanned.

Figure 2 shows the emitted LIBS spectrum for the aluminum and lead–tin alloy block—with pulse energy of 0.75 μJ and a repetition rate of 225 kHz. Here, the pulse energy is the on-target value after beam delivery loss and the same hereafter. The sample scanning speeds for Figs. 2(a) and 2(b) are 2 and 20 mm/s, and the total integration time for spectrum collection is 0.5 and 5 s, respectively. The scanning speeds and collection times were chosen differently to obtain sufficient spectrum signals. The trace in Fig. 2 represents the sums of a single spectrum from hundred of thousand laser firings. The elemental atomic peaks in the spectrum are specified in the figures—Al (309.28 and 396.16 nm), Pb (368.34 and 405.78 nm), and Sn (317.50 and 326.23 nm). It should be pointed out that some peaks lines actually represents two or more distinct peak lines, which cannot be distinguished from each other due to the poor spectral resolution of the spectrometer, and similar cases were observed for other peak wavelengths of other materials.

Figure 3 shows another representative emitted LIBS spectrum for soda lime glass and GaAs surface ablation with a pulse energy of 3.0 μJ and repetition rate of 225 kHz. The scanning speed for Figs. 3(a) and 3(b) are 4 and 20 mm/s, and the integration time are 0.5 and 0.2 s, respectively. The strong peaks in Fig. 3(a) are referring to Ca (393.36 and 396.85), Mg (517.27 and 518.36 nm), Na (588.98 nm), and K (766.49 and 769.90 nm), respectively. Here sensitivity of the CCD based LIBS is estimated to be 200 ppm from the weakest LIBS signal, element K, and its concentration. The peaks in Fig. 3(b) shown are for As (228.81 and 234.98 nm).

As shown in Figs. 2 and 3, the spectra show some radiation continuum (smooth portion on the ground)

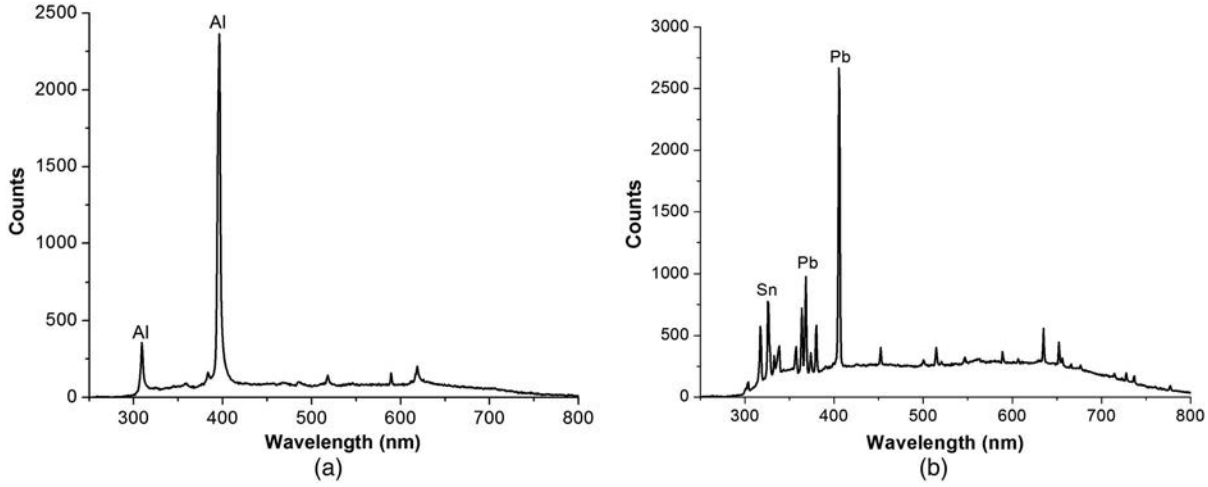

Fig. 2. LIBS signal obtained from (a) aluminum block and (b) lead–tin alloy block.

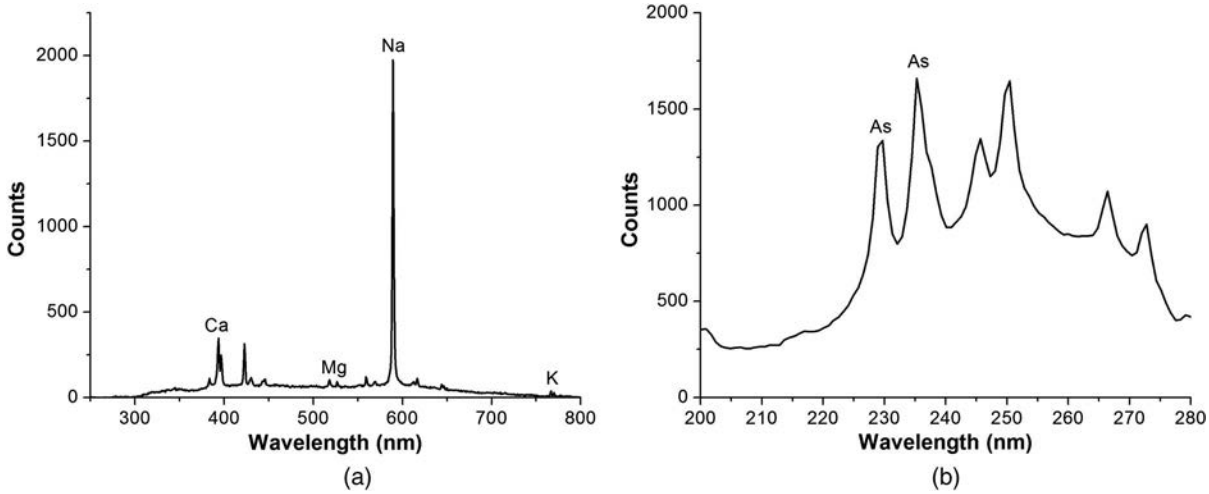

Fig. 3. LIBS signal obtained from (a) soda lime glass and (b) GaAs.

with atomic lines above. Although it is accumulated over many individual spectra, the plasma emission continuum is moderate and the SNR to the highest peak is almost in the same range compared with the value achieved by other studies using ns lasers [25,26]. It should be pointed out that there is no delay and gating control used for this experiment and the emission continuum can be largely reduced by using a delay mechanism. This suggests that nongated, nonintensified spectral acquisition without delay can be used for real time feedback and control for fs laser material processing that is cost effective and helpful especially for use in high repetition rate and high speed laser material processing.

The LIBS measurements are sensitive to many variables, including laser parameters, such as wavelength, pulse energy, pulse duration, scanning speed, pulse-to-pulse power fluctuation, and other factors such as focusing condition and ambient conditions. Here, different pulse energies and scanning speeds were investigated to study the influence of the LIBS signal.

Figures 4(a) and 4(b) shows the LIBS signal for the brass block with different pulse energies—0.75, 1.50, and 3.0 μJ from bottom to top, respectively. Other laser processing parameters are the same, including the 225 kHz repetition rate and 0.1 mm/s scanning speed. The spectrometer integration time is 0.5 s. There is pulse overlap for each spot; the pulse overlap rate is 2.25 pulses/μm, which is defined by the repetition rate over the scanning speed. The strong peaks in the spectrums are identical including Cu (324.75, 327.40, 510.55, 515.32, and 521.82 nm) and Zn (472.22 and 481.05 nm). As shown in Fig. 4(a), both the peaks and continuum signal levels are increasing with increasing pulse energy for the same scanning speed. But the SNR does not change as shown in Fig. 4(b), which means both the atomic emission and the background continuum emission increase simultaneously with the same ratio.

Figure 5 shows the LIBS signal for the brass block with different scanning speeds—0.1, 0.2, 0.4, 1.0, 2.0, 4.0, 10.0 and 20.0 mm/s from bottom to top, respectively. The other parameters are the same—225 kHz repetition rate, 3.0 μJ pulse energy and 0.5 s integration time. The same trend can be observed initially—both the peaks and continuum signal levels are increasing when the scanning speed increases from 0.1 to 10 mm/s. The signal level reaches the maximum at

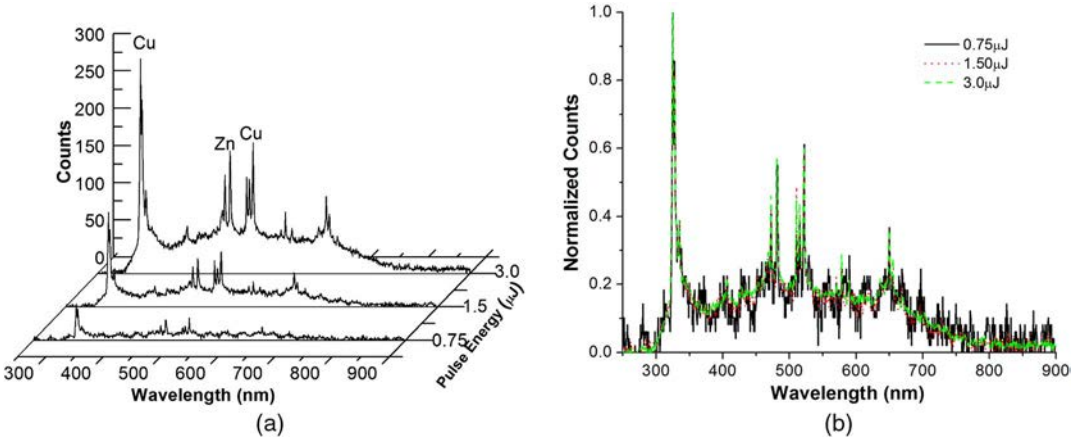

Fig. 4. (Color online) LIBS signal obtained from brass block: (a) real counts with different pulse energies—0.75, 1.5, and 3.0 μJ from bottom to top and (b) normalized counts for (a).

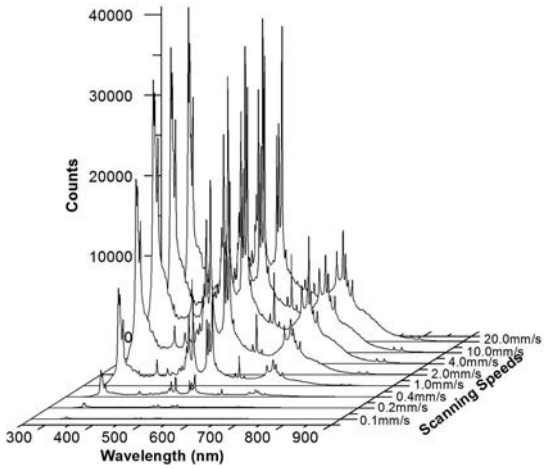

Fig. 5. LIBS signal obtained from brass block: real counts with different scanning speeds, 0.1–20.0 mm/s from bottom to top.

about 10 mm/s and is maintained when the speed changes from 10 to 20 mm/s. Furthermore, the intensity level decreases with increasing scanning speeds, from 20 mm/s and higher. This can be mostly related to the amount of material ablated. For slower scanning speeds, there are many pulse overlaps for each ablation spot, especially for scanning speed less than 1.0 mm/s. As the overlapped pulse firings generate deeper craters, the ablation depth for each pulse decreases compared with the several initial pulses. So the total ablation volume for the overlapped pulses becomes relatively smaller, reducing the atomic and background emission. However, when the scanning speed is higher, there is less or even no pulse overlap along the scanning path, so each pulse firing is incident to the location of fresh material and the ablation volume per pulse is larger than cases of slower scanning speed. This greatly increases both the atomic emission and background continuum emission. Other possible reasons include the reduced ablation efficiency due to the plasma shielding effect and the reduced signal collecting efficiency at slower scanning speeds. However, when the scanning speed is even higher, the ablation threshold will increase due to less pulse overlap [27,28] and the LIBS signal intensity will become weaker.

For comparison, the LIBS signal collected by the ICCD system was accessed with time-resolved analysis of single shot ablation. Figure 6 shows microscopic images of aluminum single shot ablation craters for different laser pulse energies. The repetition rate was changed to 1 Hz and the pulse energies are given in the figure. Actually, there does appear to be some melting. The energy threshold for plasma formation is relatively low (0.21 μJ) with this fs laser excitation compared to long-pulse excitation. The diameter of the craters increases with increasing laser pulse energy as shown in the figure. The crater size for 0.39 μJ is around 3.5 μm in diameter, less than the focal spot size, and can be smaller for even smaller pulse energy. The sub-spot-size craters show the potential for further improved spatial resolution

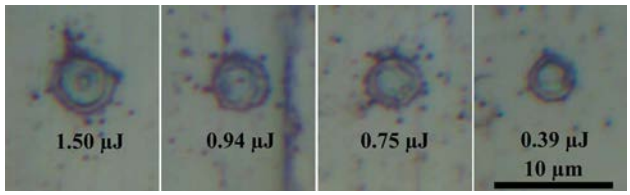

Fig. 6. (Color online) Microscopic images of aluminum ablation craters by single fs laser pulses with different pulse energies. Pulse energy is marked in the figure.

using fs lasers with a smaller focal spot size for LIBS application. Figure 7 shows the measured time-resolved LIBS result of the aluminum sample collected over the entire lifetime of the plasma using single shot ablation. The spectra were acquired with a 2.2 μJ pulse energy, 50-pulse accumulation and 5 ns gating time resolution. Before the fs laser pulse reaches the sample (−5 to 0 ns), no signal was collected. At time zero, right after the fs laser pulse reaches the sample, only a continuum spectrum (300–700 nm) was collected. This shows that for the early high temperature plasma, the plasma emits only a continuum of radiation, which does not contain any useful information about the sample. At times between 5 and 10 ns, the plasma expands at high velocities and cools, the characteristic atomic emission lines of the sample elements can be observed together with reduced continuum background. Interestingly, it is found that the intensities of the atomic lines reach a maximum at 10 ns after the termination of the laser pulse rather than at time zero that corresponds to the peak laser intensity. At times after 10 ns, the remaining plasma continues to produce only atomic emission, but the collected signal decays rapidly afterward. This also shows the shorter interaction time and fast decaying of plasma for fs laser pulses.

Compared with the LIBS results collected using a nongated, nonintensified detector, the results using gated ICCD show that the continuum emission is significantly lower and the SNR can be improved with proper delay and gate width, as shown in Fig. 7 (0–30 ns and 10–30 ns). The time-resolved spectrum measurement clearly shows that better LIBS SNR is achieved by collecting over 10–30 ns and the SNR for the 396.15 nm Al emission line over 10–30 ns is improved by a factor of 3 compared with the spectrum collected over 0–30 ns. This represents the great advantage of utilizing delay and gating for LIBS.

Figure 8 shows the time-resolved emission results of the soda lime glass using single shot ablation. The pulse energy and number of pulse accumulation are the same as Fig. 7. Similarly, the plasma emission shows the same trend as the aluminum in Fig. 7 and the plasma lifetime of the soda lime glass is close to that of aluminum. But, as shown in Fig. 8, the continuum background at 5 ns is obviously lower and the possible reason is the less conductive and non-absorbing material properties of the soda lime glass. Meanwhile, it is also worth mentioning that the atomic emission line with a relatively higher energy level (shorter wavelength) was emitted at the earlier

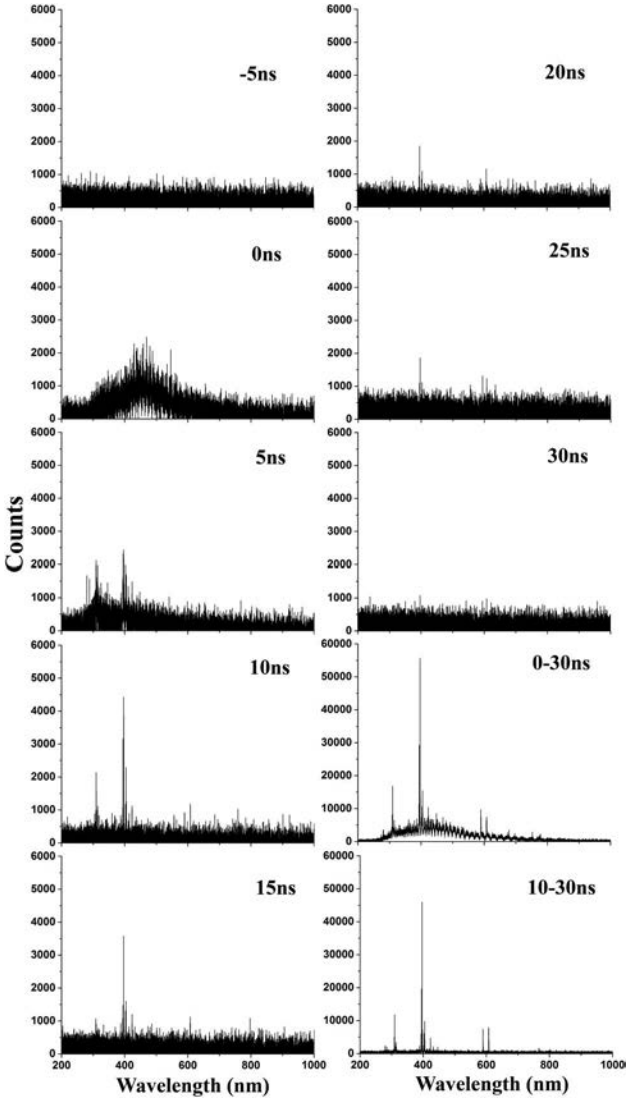

Fig. 7. Time-resolved LIBS signal measured from aluminum block with 5 ns gate width. Delay time or gated width is marked in each figure.

stage of the plasma lifetime; the atomic line with lower energy (longer wavelength) can be seen at the later stage of the emission.

Figure 9 compares the LIBS results of the brass block from the CCD and ICCD. The result from the CCD was obtained with a 225 kHz repetition rate, 0.1 mm/s scanning speed, 2.2 μJ pulse energy, and 0.5 s integration time. The result from the ICCD was obtained using single shot ablation with a 50-pulse accumulation, and the same pulse energy. The delay and gate width is 10 and 20 ns, respectively. The SNR for the 324.75 nm Cu emission line by the ICCD system is over 800∶1 and has an approximate factor-of-20 improvement compared with the SNR by the CCD system. This is consistent with recently published results [26,29], where it is found that the SNR of a gated detection ICCD system is better than that of a nongated CCD system by a factor of 10–100. The estimated sensitivity can be improved to 10 ppm level accordingly for K element in soda lime glass.

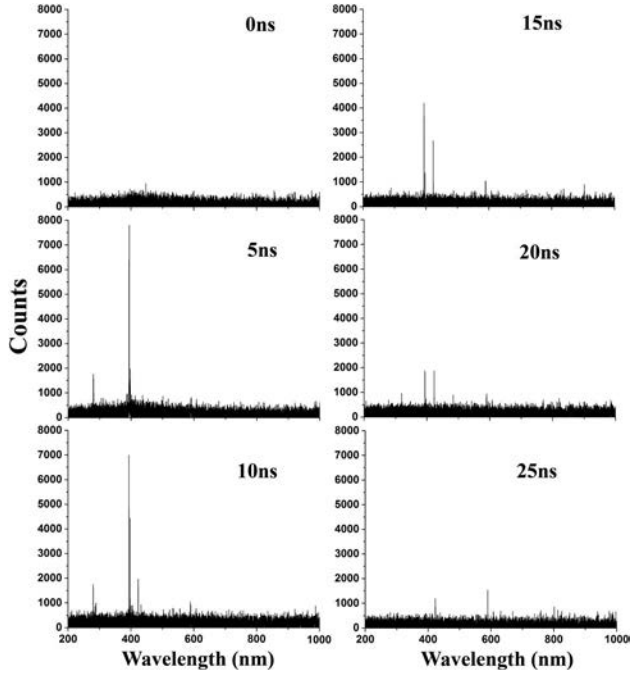

Fig. 8. Time-resolved LIBS signal measured from soda lime glass with 5 ns gate width. Delay time is marked in each time step.

Both detectors can give the atomic emission line information successfully and are practical technologies for LIBS application. This provides the researcher with a range of detector options to match specific applications. The result from the ICCD shows very good SNR and the continuum background base is almost removed with proper delay and gating control. This is useful in applications that require rapid sorting or those that prefer emission from a single particle. But it has the disadvantage of high cost and low level field deployability. A nonintensified detector is advantageous because of its lower cost and compact size. So, it can be integrated into portable LIBS systems together with a compact fs fiber laser. Meanwhile, it can be used for real-time feedback and control for laser processing systems.

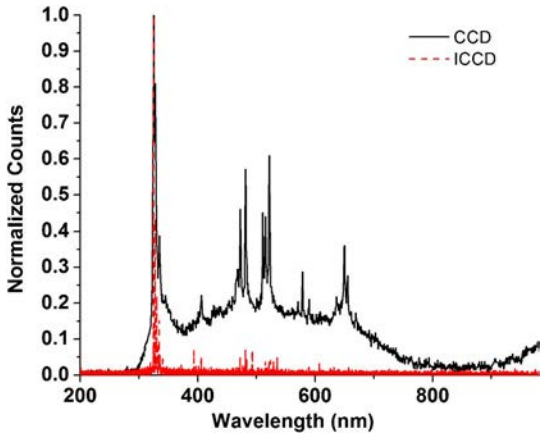

Fig. 9. (Color online) LIBS comparison results of brass block with CCD and ICCD.

4. Conclusion and Outlook

Elemental composition detection and identification by utilizing an fs fiber laser at atmospheric pressure have been demonstrated. Qualitative LIBS spectra were obtained using relatively low pulse energy and the emission lines of different materials including metals, metal alloys, semiconductor and glass have been characterized using both CCD and ICCD detectors. Different laser parameters, including scanning speed and pulse energy, have been studied to investigate their influence. Results show that faster scanning speed and higher pulse energies can enhance the signal level. Thus, it is possible that a nongated, nonintensified CCD detector can be used for real-time feedback and processing control by collecting LIBS spectra for laser materials processing, such as cutting, thin film scribing, and multi layer removing. Time-resolved emission spectra depicting the detailed plasma evolution was collected from sub-spot-size craters, which shows the potential for further improved spatial resolution using fs laser for LIBS application. The gated ICCD gives an improved SNR by a factor of 20 compared with a nongated, nonintensified CCD system. This can lead to a portable and field-deployable LIBS detection system utilizing reliable, compact, and low cost fs fiber laser systems.

Future works with this fs fiber laser based LIBS technique include the investigation of laser parameters to enhance the spatial resolution and SNR ratio and quantification studies of different materials.

This work was partially funded by NSF and U.S. Army SBIR programs.

References

1. V. Margetic, A. Pakulev, A. Stockhaus, M. Bolshov, K. Niemax, and R. Hergenröder, "A comparison of nanosecond and femtosecond laser-induced plasma spectroscopy of brass samples," Spectrochim. Acta, Part B **55**, 1771–1785 (2000).
2. D. J. Hwang, H. Jeon, C. P. Grigoropoulos, J. Yoo, and R. E. Russo, "Femtosecond laser ablation induced plasma characteristics from submicron craters in thin metal film," Appl. Phys. Lett. **91**, 251118–251113 (2007).
3. M. Sabsabi and P. Cielo, "Quantitative analysis of aluminum alloys by laser-induced breakdown spectroscopy and plasma characterization," Appl. Spectrosc. **49**, 499–507 (1995).
4. C. Geertsen, J. L. Lacour, P. Mauchien, and L. Pierrard, "Evaluation of laser ablation optical emission spectrometry for microanalysis in aluminium samples," Spectrochim. Acta Part B **51**, 1403–1416 (1996).
5. H. Bette and R. Noll, "High speed laser-induced breakdown spectrometry for scanning microanalysis," J. Phys. D **37**, 1281–1288 (2004).
6. R. Sattmann, I. Monch, H. Krause, R. Noll, S. Couris, A. Hatziapostolou, A. Mavromanolakis, C. Fotakis, E. Larrauri, and R. Miguel, "Laser-induced breakdown spectroscopy for polymer identification," Appl. Spectrosc. **52**, 456–461 (1998).
7. M. Baudelet, L. Guyon, J. Yu, J. P. Wolf, T. Amodeo, E. Fréjafon, and P. Laloi, "Femtosecond time-resolved laser-induced breakdown spectroscopy for detection and identification of bacteria: a comparison to the nanosecond regime," J. Appl. Phys. **99**, 084701–084709 (2006).
8. A. Assion, M. Wollenhaupt, L. Haag, F. Mayorov, C. Sarpe-Tudoran, M. Winter, U. Kutschera, and T. Baumert, "Femtosecond laser-induced-breakdown spectrometry for Ca 2+ analysis of biological samples with high spatial resolution," Appl. Phys. B **77**, 391–397 (2003).
9. A. Kumar, F. Y. Yueh, J. P. Singh, and S. Burgess, "Characterization of malignant tissue cells by laser-induced breakdown spectroscopy," Appl. Opt. **43**, 5399–5403 (2004).
10. A. Ball, V. Hohreiter, and D. Hahn, "Hydrogen leak detection using laser-induced breakdown spectroscopy," Appl. Spectrosc. **59**, 348–353 (2005).
11. M. Tran, B. W. Smith, D. W. Hahn, and J. D. Winefordner, "Detection of gaseous and particulate fluorides by laser-induced breakdown spectroscopy," Appl. Spectrosc. **55**, 1455–1461 (2001).
12. F. C. De Lucia, J. L. Gottfried, and A. W. Miziolek, "Evaluation of femtosecond laser-induced breakdown spectroscopy for explosive residue detection," Opt. Express **17**, 419–425 (2009).
13. F. C. De Lucia, J. L. Gottfried, C. A. Munson, and A. W. Miziolek, "Multivariate analysis of standoff laser-induced breakdown spectroscopy spectra for classification of explosive-containing residues," Appl. Opt. **47**, G112–G121 (2008).
14. C. Brown, M. Baudelet, C. Bridge, M. Fisher, M. Sigman, P. Dagdigian, and M. Richardson, "Atmosphere issues in detection of explosives and organic residues," Proc. SPIE **7304**, 73041D (2009).
15. Y. Dikmelik, C. McEnnis, and J. B. Spicer, "Femtosecond and nanosecond laser-induced breakdown spectroscopy of trinitrotoluene," Opt. Express **16**, 5332–5337 (2008).
16. K. Amal, S. Elnaby, V. Palleschi, A. Salvetti, and M. Harith, "Comparison between single-and double-pulse LIBS at different air pressures on silicon target," Appl. Phys. B **83**, 651–657 (2006).
17. R. Sattmann, V. Sturm, and R. Noll, "Laser-induced breakdown spectroscopy of steel samples using multiple *Q*-switch Nd:YAG laser pulses," J. Phys. D **28**, 2181 (1999).
18. M. E. Asgill, M. S. Brown, K. Frische, W. M. Roquemore, and D. W. Hahn, "Double-pulse and single-pulse laser-induced breakdown spectroscopy for distinguishing between gaseous and particulate phase analytes," Appl. Opt. **49**, C110–C119 (2010).
19. B. Le Drogoff, M. Chaker, J. Margot, M. Sabsabi, O. Barthélemy, T. Johnston, S. Laville, and F. Vidal, "Influence of the laser pulse duration on spectrochemical analysis of solids by laser-induced plasma spectroscopy," Appl. Spectrosc. **58**, 122–129 (2004).
20. A. Semerok, C. Chaléard, V. Detalle, J. L. Lacour, P. Mauchien, P. Meynadier, C. Nouvellon, B. Sallé, P. Palianov, and M. Perdrix, "Experimental investigations of laser ablation efficiency of pure metals with femto, pico and nanosecond pulses," Appl. Surf. Sci. **138**, 311–314 (1999).
21. B. Le Drogoff, J. Margot, M. Chaker, M. Sabsabi, O. Barthelemy, T. Johnston, S. Laville, F. Vidal, and Y. Von Kaenel, "Temporal characterization of femtosecond laser pulses induced plasma for spectrochemical analysis of aluminum alloys," Spectrochim. Acta Part B **56**, 987–1002 (2001).
22. M. R. Leahy-Hoppa, J. Miragliotta, R. Osiander, J. Burnett, Y. Dikmelik, C. McEnnis, and J. B. Spicer, "Ultrafast laser-based spectroscopy and sensing: applications in LIBS, CARS, and THz spectroscopy," Sensors **10**, 4342–4372 (2010).
23. M. Baudelet, C. Willis, L. Shah, and M. Richardson, "Laser-induced breakdown spectroscopy of copper with a 2 microm thulium fiber laser," Opt. Express **18**, 7905 (2010).
24. J. F. Y. Gravel, F. R. Doucet, P. Bouchard, and M. Sabsabi, "Evaluation of a compact high power pulsed fiber laser source for laser-induced breakdown spectroscopy," J. Anal. At. Spectrom. **26**, 1354–1361 (2011).
25. B. T. Fisher, H. A. Johnsen, S. G. Buckley, and D. W. Hahn, "Temporal gating for the optimization of laser-induced breakdown spectroscopy detection and analysis of toxic metals," Appl. Spectrosc. **55**, 1312–1319 (2001).

26. J. E. Carranza, E. Gibb, B. W. Smith, D. W. Hahn, and J. D. Winefordner, "Comparison of nonintensified and intensified CCD detectors for laser-induced breakdown spectroscopy," Appl. Opt. **42**, 6016–6021 (2003).
27. S. Baudach, J. Bonse, and W. Kautek, "Ablation experiments on polyimide with femtosecond laser pulses," Appl. Phys. A **69**, S395–S398 (1999).
28. H. Huang and Z. Guo, "Ultra-short pulsed laser PDMS thin-layer separation and micro-fabrication," J. Micromech. Microeng. **19**, 055007 (2009).
29. M. Sabsabi, R. Heon, and L. St-Onge, "Critical evaluation of gated CCD detectors for laser-induced breakdown spectroscopy analysis," Spectrochim. Acta Part B **60**, 1211–1216 (2005).